

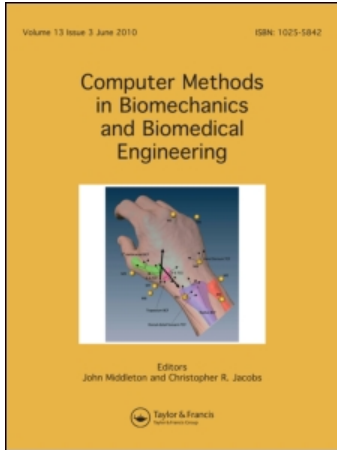
This article was downloaded by: [University Of British Columbia]

On: 20 July 2010

Access details: Access Details: [subscription number 917249135]

Publisher Taylor & Francis

Informa Ltd Registered in England and Wales Registered Number: 1072954 Registered office: Mortimer House, 37-41 Mortimer Street, London W1T 3JH, UK



## Computer Methods in Biomechanics and Biomedical Engineering

Publication details, including instructions for authors and subscription information:

<http://www.informaworld.com/smpp/title~content=t713455284>

### Predicting muscle patterns for hemimandibulectomy models

Ian Stavness<sup>a</sup>; Alan G. Hannam<sup>b</sup>; John E. Lloyd<sup>a</sup>; Sidney Fels<sup>a</sup>

<sup>a</sup> Department of Electrical and Computer Engineering, University of British Columbia, Vancouver, BC, Canada <sup>b</sup> Faculty of Dentistry, University of British Columbia, Vancouver, BC, Canada

Online publication date: 15 July 2010

**To cite this Article** Stavness, Ian , Hannam, Alan G. , Lloyd, John E. and Fels, Sidney(2010) 'Predicting muscle patterns for hemimandibulectomy models', Computer Methods in Biomechanics and Biomedical Engineering, 13: 4, 483 — 491

**To link to this Article:** DOI: 10.1080/10255841003762034

**URL:** <http://dx.doi.org/10.1080/10255841003762034>

PLEASE SCROLL DOWN FOR ARTICLE

Full terms and conditions of use: <http://www.informaworld.com/terms-and-conditions-of-access.pdf>

This article may be used for research, teaching and private study purposes. Any substantial or systematic reproduction, re-distribution, re-selling, loan or sub-licensing, systematic supply or distribution in any form to anyone is expressly forbidden.

The publisher does not give any warranty express or implied or make any representation that the contents will be complete or accurate or up to date. The accuracy of any instructions, formulae and drug doses should be independently verified with primary sources. The publisher shall not be liable for any loss, actions, claims, proceedings, demand or costs or damages whatsoever or howsoever caused arising directly or indirectly in connection with or arising out of the use of this material.

## Predicting muscle patterns for hemimandibulectomy models

Ian Stavness<sup>a\*</sup>, Alan G. Hannam<sup>b</sup>, John E. Lloyd<sup>a</sup> and Sidney Fels<sup>a</sup>

<sup>a</sup>Department of Electrical and Computer Engineering, University of British Columbia, Vancouver, BC, Canada; <sup>b</sup>Faculty of Dentistry, University of British Columbia, Vancouver, BC, Canada

(Received 13 August 2009; final version received 14 February 2010)

Deficits in movement and bite force are common in patients following segmental resection of the mandible consequent to oral cancer or injury. We have previously developed a dynamic model to analyse the biomechanics of an ungrafted segmental jaw resection with unilateral muscle and joint loss and post-surgical scarring. Here, we describe an inverse-modelling algorithm for automatically predicting muscle activations in the model for prescribed jaw movement and bite-force production. We present the results of simulations that postulate combined muscle activation patterns that could theoretically be used by patients to overcome post-surgical deficits. Such predictions could be the basis for future muscle retraining in clinical cases.

**Keywords:** biomechanics simulation; inverse modelling; muscle forces; optimisation; dynamic jaw modelling; hemimandibulectomy

### 1. Introduction

Segmental resection and reconstruction of the mandible can result in the permanent loss of some jaw muscles, altered articular function and significant soft-tissue scarring, all of which can be expected to affect system biomechanics. Depending upon the extent of the resection, post-operative deficits have been reported in jaw movement, bite-force generation and mastication (Urken et al. 1991; Marunick et al. 1992; Schmelzeisen et al. 1996; Curtis et al. 1997; Roumanas et al. 2006). There are compelling reasons for defining what is physically possible for a patient, and whether particular patterns of muscle use could be employed to compensate for given deficiencies.

Recently, we have been using forward-dynamics modelling to analyse jaw function with and without mandibular continuity (Hannam et al. 2010). Simulated external forces on the jaw and muscle activation, either singly or in groups, have provided insight into the movement patterns and jaw instabilities seen clinically. A particular instance is the resting jaw's posture after hemimandibulectomy, which is deviated to the side of the deficit accompanied by rotation of the mandible when viewed frontally.

Without experimental data upon which to base muscle input, however, forward-dynamic simulations require trial-and-error approaches to determine whether a particular jaw posture or movement can be attained by activating the remaining jaw muscles. Here, we describe an alternative method based on inverse dynamics, to reveal

the muscle forces needed to maintain a midline jaw resting posture and to perform unilateral clenching in a mandible without continuity.

Model-based predictions of muscle forces during movement have been proposed for a variety of musculoskeletal systems because muscle force is difficult to measure *in vivo* (Erdemir et al. 2007). Electromyography (EMG) involves transducing electrical signals associated with muscle activation; however, EMG can be difficult to record for small, deep muscles in the head and neck, and the relationship between EMG and muscle force is complex for dynamic movements (Sherif et al. 1983). Movement and contact forces are easier to measure directly than muscle forces, making model-based inverse techniques which predict muscle forces from kinematic records an attractive option in future clinical experiments.

Our approach to predicting patterns of muscle activation is classified in Erdemir et al. (2007) as 'forward dynamics assisted data tracking'. We formulate an optimisation to predict muscle activations that drive the system's forward dynamics through a prescribed target movement trajectory. A computationally efficient algorithm to solve the movement tracking problem has been proposed for gait analysis (Thelen and Anderson 2006) and hand animation (Sueda et al. 2008). Here, we extend this approach to include constraint force targets in addition to movement targets. The constraint force targets are used to predict muscle activations needed to generate desired reaction forces in the system, such as a target bite force during unilateral tooth clenching.

\*Corresponding author. Email: stavness@ece.ubc.ca

## 2. Material and methods

### 2.1 Inverse-dynamics tracking algorithm

The tracking algorithm was implemented within the ArtiSynth biomechanics simulation toolkit ([www.artisynth.org](http://www.artisynth.org), Department of Electrical and Computer Engineering, University of British Columbia, Vancouver, Canada; and see Fels et al. (2009)). ArtiSynth is designed to simulate the dynamics of hard and soft-tissue structures using coupled rigid-body and finite-element models (FEMs).

Within ArtiSynth, a mechanical system consists of an assembly of rigid bodies and particles (which include FEM nodes). Let  $\mathbf{x}$ ,  $\mathbf{v}$  and  $\mathbf{f}$  denote the composite position, velocity and force vectors for these components, and let  $\mathbf{f}$  be partitioned into  $\mathbf{f} = \mathbf{f}_p + \mathbf{f}_a$ , where  $\mathbf{f}_p$  are the passive forces arising from muscle stretch, ligaments and scar tissue, and  $\mathbf{f}_a$  are the active forces arising from muscle activation. The system's dynamic behaviour is then determined by Newton's second law:

$$\mathbf{M}\dot{\mathbf{v}} = \mathbf{f}(\mathbf{x}, \mathbf{v}, t) = \mathbf{f}_p(\mathbf{x}, \mathbf{v}) + \mathbf{f}_a(\mathbf{x}, \mathbf{v}, \mathbf{a}(t)), \quad (1)$$

where  $\mathbf{M}$  is a block-diagonal mass matrix.

We use Hill-type muscle models that are linear in activation and non-linearly dependent on the length and shortening velocity, so that

$$\mathbf{f}_a = \mathbf{A}(\mathbf{x}, \mathbf{v})\mathbf{a},$$

where  $\mathbf{a}$  is a vector of activation levels bounded between 0 and 100% for each muscle. The matrix  $\mathbf{A}$  relates muscle activations to system forces and can be determined either analytically or numerically; we currently use an analytic formulation. We neglect the calcium-dependent activation dynamics of muscle tissue, which are typically modelled as a first-order low-pass filter (Zajac 1989). The consequence of this assumption is that predicted muscle forces could change faster than physiologically possible; however, this was not found to occur for target movements with physiologically plausible velocities.

The mechanical system may also contain bilateral and unilateral constraints; the former include articulating joints between rigid bodies and FEM incompressibility, while the latter include contact conditions and joint limits. Unilateral constraints are not considered in this paper (as discussed in Section 4), but we do utilise bilateral constraints, which take the form of linear equality constraints on the velocity:

$$\mathbf{G}(\mathbf{x})\mathbf{v} = 0. \quad (2)$$

Differentiating this also leads to acceleration constraints

$$\mathbf{G}(\mathbf{x})\dot{\mathbf{v}} = \mathbf{g}, \quad \mathbf{g} \equiv -\dot{\mathbf{G}}\mathbf{v}. \quad (3)$$

For example, to constrain one point of a rigid body to a planar surface, a constraint is formed to prevent

translation of the point normal to the plane, i.e.  $\mathbf{G} = (n_x, n_y, n_z, 0, 0, 0)$ , where  $(n_x, n_y, n_z)$  is the normal vector of the plane.

Constraints are enforced by forces applied to  $\mathbf{G}^T$ , so that (1) becomes

$$\mathbf{M}\dot{\mathbf{v}} = \mathbf{f}_p(\mathbf{x}, \mathbf{v}) + \mathbf{A}(\mathbf{x}, \mathbf{v})\mathbf{a} + \mathbf{G}^T(\mathbf{x})\lambda, \quad (4)$$

where  $\lambda$  are Lagrange multipliers giving the magnitudes of the constraint reaction forces.

Solving the system dynamics involves integrating (4) forward in time. At present, this is done using a first-order integrator that is semi-implicit with respect to the passive forces  $\mathbf{f}_p$  (which are often stiff). Letting  $h$  equal the timestep, and using a superscript to denote values at step  $i$ , this leads to

$$\mathbf{M}\mathbf{v}^{i+1} = \mathbf{M}\mathbf{v}^i + h\mathbf{f}_p^{i+1}(\mathbf{x}, \mathbf{v}) + h\mathbf{A}^i(\mathbf{x}, \mathbf{v})\mathbf{a} + \mathbf{G}^{iT}(\mathbf{x})\lambda, \quad (5)$$

where  $\lambda$  now denotes constraint impulses.  $\mathbf{f}_p^{i+1}$  is approximated using

$$\begin{aligned} \mathbf{f}_p^{i+1} &\approx \mathbf{f}_p^i + \frac{\partial \mathbf{f}_p}{\partial \mathbf{x}} \Delta \mathbf{x} + \frac{\partial \mathbf{f}_p}{\partial \mathbf{v}} \Delta \mathbf{v} \\ &= \mathbf{f}_p^i + \frac{\partial \mathbf{f}_p}{\partial \mathbf{x}} h\mathbf{v}^{i+1} + \frac{\partial \mathbf{f}_p}{\partial \mathbf{v}} (\mathbf{v}^{i+1} - \mathbf{v}^i). \end{aligned}$$

Combining this with (5) and (3) leads to the system

$$\begin{pmatrix} \hat{\mathbf{M}} & -\mathbf{G}^T \\ \mathbf{G} & \mathbf{0} \end{pmatrix} \begin{pmatrix} \mathbf{v}^{i+1} \\ \lambda \end{pmatrix} = \begin{pmatrix} \mathbf{M}\mathbf{v}^i + h\hat{\mathbf{f}}_p + h\mathbf{A}\mathbf{a} \\ \mathbf{g} \end{pmatrix}, \quad (6)$$

where

$$\hat{\mathbf{M}} \equiv \left( \mathbf{M} - h \frac{\partial \mathbf{f}_p}{\partial \mathbf{v}} - h^2 \frac{\partial \mathbf{f}_p}{\partial \mathbf{x}} \right) \quad \text{and} \quad \hat{\mathbf{f}}_p \equiv \mathbf{f}_p^i - \frac{\partial \mathbf{f}_p}{\partial \mathbf{v}} \mathbf{v}^i$$

are the mass matrix and force term augmented with Jacobian terms required for the implicit solve. Unlike  $\mathbf{M}$ ,  $\hat{\mathbf{M}}$  is neither block diagonal nor symmetric positive definite, but it is sparse and (for the applications considered in this paper) symmetric.

Solving for  $\lambda$  in Equation (6) we find

$$\lambda = (\mathbf{G}\hat{\mathbf{M}}^{-1}\mathbf{G}^T)^{-1}\mathbf{g} - \mathbf{Q}(\mathbf{k} + h\mathbf{A}\mathbf{a}), \quad (7)$$

where  $\mathbf{Q} \equiv (\mathbf{G}\hat{\mathbf{M}}^{-1}\mathbf{G}^T)^{-1}\hat{\mathbf{M}}^{-1}$  and  $\mathbf{k} \equiv \mathbf{M}\mathbf{v}^i + h\hat{\mathbf{f}}_p$ . Back substituting for  $\lambda$  and solving for  $\mathbf{v}^{i+1}$  in Equation (6) yields

$$\mathbf{v}^{i+1} = \mathbf{Q}^T\mathbf{g} + \hat{\mathbf{M}}^{-1}\mathbf{P}_f(\mathbf{k} + h\mathbf{A}\mathbf{a}), \quad (8)$$

where  $\mathbf{P}_f \equiv (\mathbf{I} - \mathbf{G}^T\mathbf{Q})$  is a matrix that projects forces into the range compatible with the constraints  $\mathbf{G}$ , and  $\mathbf{Q}^T = \hat{\mathbf{M}}^{-1}\mathbf{G}^T(\mathbf{G}\hat{\mathbf{M}}^{-1}\mathbf{G}^T)^{-1}$  (by the symmetry of  $\hat{\mathbf{M}}$ ). Equations (7) and (8) relate muscle activations to future constraint

forces and velocities and can be used to formulate an optimisation over muscle activations with a cost function that includes desired movement and constraint force goals.

The *movement goal* of the algorithm is given as a target velocity trajectory  $\mathbf{v}^*$ , and we desire to find muscle activations that minimise  $(1/2)\|\mathbf{v}^* - \mathbf{v}^{i+1}\|^2$ . Substituting for  $\mathbf{v}^{i+1}$  from Equation (8), the optimisation term for the movement target can be expressed as a quadratic form in  $\mathbf{a}$ :

$$\phi_m(\mathbf{a}) = \frac{1}{2}\|\bar{\mathbf{v}} - \mathbf{H}_m\mathbf{a}\|^2, \quad (9)$$

where  $\bar{\mathbf{v}} \equiv \mathbf{v}^* - \mathbf{Q}^T\mathbf{g} - \hat{\mathbf{M}}^{-1}\mathbf{P}_f\mathbf{k}$  and  $\mathbf{H}_m \equiv h\hat{\mathbf{M}}^{-1}\mathbf{P}_f\mathbf{A}$ . For a rigid body, such as the jaw, the target movement can be specified as either the full 6D position and orientation of the body, the 3D position of a single point on the body (in which case the body's motion is partly unconstrained), or the 3D position of multiple points on the body (in which case a best least-squares fit to the points is used). Target velocities can be computed from the target position trajectory at each timestep providing online correction to position errors.

The *constraint force goal* is given as target values for Lagrange multipliers,  $\lambda$ , which are the magnitudes of the constraint reaction impulses. Given target constraint forces  $\xi$ , the corresponding impulses are  $h\xi$  and so we desire to find muscle activations that minimise  $(1/2)\|h\xi - \lambda\|^2$ , which leads to a second term in the optimisation cost function which is also a quadratic form in  $\mathbf{a}$ :

$$\phi_c(\mathbf{a}) = \frac{1}{2}\|\bar{\lambda} - \mathbf{H}_c\mathbf{a}\|^2, \quad (10)$$

where  $\bar{\lambda} \equiv h\xi - (\mathbf{G}\hat{\mathbf{M}}^{-1}\mathbf{G}^T)^{-1}\mathbf{g} + \mathbf{Q}\mathbf{k}$  and  $\mathbf{H}_c \equiv -h\mathbf{Q}\mathbf{A}$ .

We can selectively include a subset of the constraints into the optimisation term. Static clenching is achieved by specifying a constant movement target and a non-zero force target on the bite constraint. The bite constraint is modelled as a planar constraint surface, and therefore has a single constraint dimension and a scalar Lagrange multiplier.

The optimisation problem is underdetermined for a biomechanical system with redundant muscle activations. We include a weighted  $\ell^2$ -norm regularisation term,  $(1/2)\mathbf{a}^T\mathbf{W}^{-1}\mathbf{a}$ , where  $\mathbf{W}$  is a diagonal matrix of muscle cross-sectional areas, in order to select the most efficient set of activations (Ait-Haddou et al. 2004). Other regularisation terms may be used within our formulation, such as an  $\ell^1$ -norm term,  $\|\mathbf{a}\|_1$ , to select the smallest set of non-zero activations or a damping term,  $(1/2)\|\mathbf{a} - \mathbf{a}^{i-1}\|^2$ , to enforce smooth activations.

Combining the movement and constraint force goals, regularisation and muscle activations bounds, we arrive at the complete optimisation problem, which takes the form

of a quadratic programme:

$$\begin{aligned} \min_{\mathbf{a}} \quad & w_m\phi_m(\mathbf{a}) + w_c\phi_c(\mathbf{a}) + \frac{w_a}{2}\mathbf{a}^T\mathbf{W}^{-1}\mathbf{a} \\ \text{subject to} \quad & 0 \leq \mathbf{a} \leq 1, \end{aligned} \quad (11)$$

where  $w_m$ ,  $w_c$  and  $w_a$  are weights used to trade-off between cost terms. For all simulations, the weights were set to  $w_m = 1$ ,  $w_c = 1$  and  $w_a = 0.1$  so that minimising tracking error was preferred over small activations.

The inverse dynamics optimisation is solved at each timestep to provide muscle activations to the forward dynamics simulation. The hemimandibulectomy model considered in this paper contains only one rigid body; however, other biomechanics models, especially those that include FEM models, can have many dynamic components resulting in a large, sparse KKT system in Equation (6). We use the KKT system solver in ArtiSynth to compute  $\bar{\mathbf{v}}$  and  $\bar{\lambda}$  as well as  $\mathbf{H}_m$  and  $\mathbf{H}_c$ , which are formed by solving the system for each column of  $\mathbf{A}$ . The resulting quadratic programme is dense but tends to be small since its dimension is the size of  $\mathbf{a}$ , i.e. the number of activations being solved for. The quadratic programme is also convex, which means it can be solved as a linear complementarity problem, which is done using an implementation of the Cottle–Dantzig algorithm (Cottle et al. 1992) contained in ArtiSynth.

## 2.2 Model

The hemimandibulectomy model is depicted in Figure 1 and is based on a previous model of the intact jaw system (Hannam et al. 2008) with modifications including resection of the mandible proximal to the left canine, removal of the left joint constraint, removal of a number of left-side muscles and the addition of a damped spring to simulate soft-tissue scarring. The inertial properties of the mandible fragment were computed based on its new shape resulting in a new mass of 126 g from 200 g for the normal jaw and a new centre-of-mass shifted from midline in the normal jaw to inside the body of the fragment inferior to the second molar.

The intact muscle groups included the right anterior, middle and posterior temporalis (RAT, RMT and RPT), right deep and superficial masseter (RDM and RSM), right medial pterygoid (RMP), right superior and inferior lateral pterygoid (RSP and RIP), right mylohyoid (RMY), right and left geniohyoid (RGH and LGH) and right and left digastric (RDI and LDI) muscles. Hill-type muscle models simulated individual muscle cross-sectional areas and length–tension properties and produced passive forces proportional to muscle stretch and active forces proportional to muscle activation. Muscle cross-sectional areas are based on previous studies of jaw (Peck et al. 2000) and floor-of-mouth muscles (Buchillard et al. 2009) and are listed in Table 1.

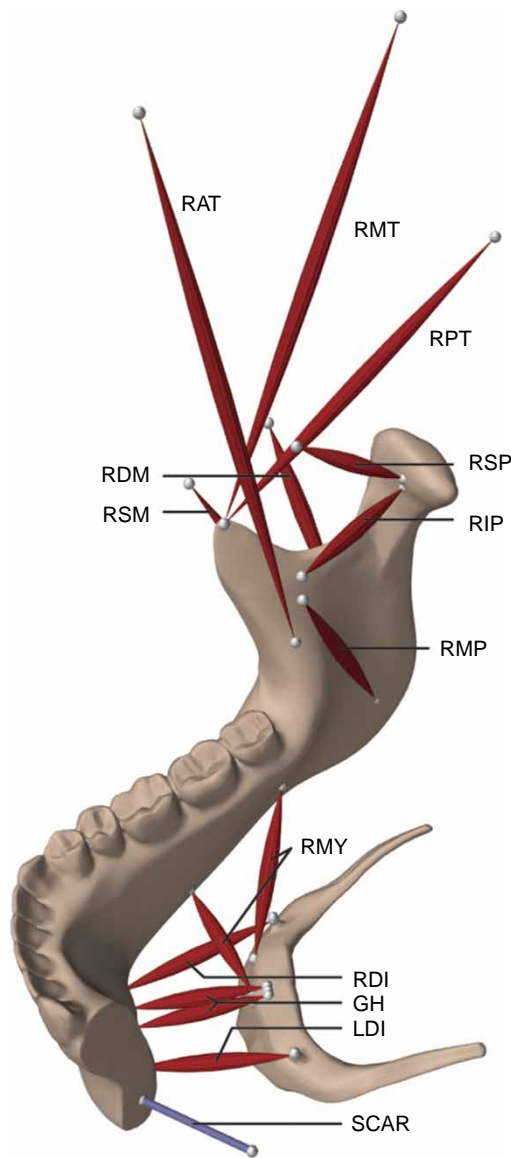


Figure 1. A model of the jaw after segmental resection with unilateral muscle and joint loss. Intact muscle groups included the RAT, RMT and RPT, RDM and RSM, RMP, RSP and RIP, RMY, RGH and LGH, RDI and LDI muscles. The effect of post-operative scarring is represented by the SCAR spring element.

The intact joint was modelled as a bilateral constraint surface, curvilinear in the anterior–posterior direction to represent the articular fossa and eminence, with no medio-lateral constraint. A posterior constraint was

included to represent the posterior aspect of the articular fossa. In all simulations, the joint worked in compression, i.e. the forces in the system never worked to pull the joint apart; therefore, it was modelled with bilateral constraints as shown in Equation (6). For clenching simulations, we added an additional planar constraint at the right first molar to simulate tooth contact.

Passive soft-tissue forces representing scarring were modelled with a linear spring with 200 N/m stiffness that drew the end of jaw fragment backwards, downwards and towards the left-side from its initial location in the intercuspal position (IP). The hyoid was fixed in the model, which would be achieved by activation of infrahyoid muscles to stiffen the hyoid; hyoid movement in hemimandibulectomy patients has not been reported, but likely differs from normal subjects due to missing muscle and scar tissue on the affected side.

### 2.3 Hinge movement simulations

Lateral deviation of a segmental jaw fragment towards the affected side during opening is likely due to the effect of post-operative scarring and the unilateral loss of the lateral pterygoid muscles (Schmelzeisen et al. 1996; Roumanas et al. 2006). We were interested in determining the muscle forces needed for midline jaw movements with the model. Therefore, we simulated movement between three jaw postures that are illustrated in Figure 2:

- REST a relaxed rest posture deviated towards the affected side and rotated clockwise in the frontal-plane.
- OPEN a midline opening posture with 20 mm interincisal separation and no frontal-plane rotation, a typically maximal opening gape during chewing.
- CLOSE a midline posture with the jaw closed to just before first tooth contact.

Two movement simulations were performed: from REST to OPEN moving the jaw fragment from the deviated rest posture to the midline, and from OPEN to CLOSE moving the jaw fragment in centric relation relative to the maxilla, for a ‘hinge-like’ movement with no frontal-plane rotation. Smooth target position trajectories were generated with quintic splines from the start posture to the end posture over a 0.5 s duration. The target velocity trajectories were computed online with finite-differencing

Table 1. Physiological cross-sectional area for remaining jaw muscles.

<i>Jaw closer muscles</i>							
Name	RAT	RMT	RPT	RSM	RDM	RMP	
CSA (mm <sup>2</sup> )	395	239	189	476	204	437	
<i>Jaw opener muscles</i>							
Name	RSP	RIP	LDI	RDI	RMY	LGH	RGH
CSA (mm <sup>2</sup> )	72	167	100	100	88	80	80

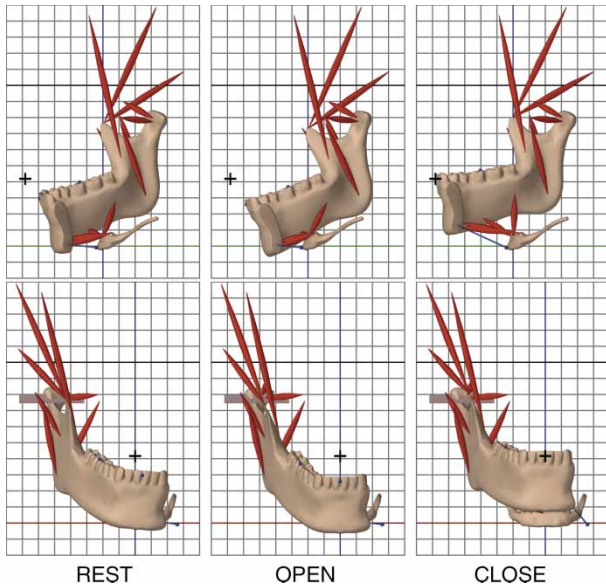


Figure 2. Sagittal and frontal-plane views of the jaw postures for relaxed rest (REST), 20 mm retrusive midline open (OPEN) and retrusive midline close to before tooth contact (CLOSE). The lower mid-incisor point at IP is denoted by +. Grid spacing is 10 mm.

which provided online correction of position errors as the simulation progressed. We specified the full six degrees-of-freedom position trajectory of the jaw in order to control its orientation. The target trajectories referenced to the 3D incisor point movement are shown for REST-to-OPEN in Figure 3(A) and for OPEN-to-CLOSE in Figure 4(A).

#### 2.4 Unilateral clench simulations

Forward dynamics simulations activating individual closer muscles in isolation illustrate that unilateral clenching with a segmental jaw fragment is a potentially unstable act. The jaw fragment exhibits large frontal-plane rotations; either clockwise due to masseter activity or counter-clockwise due to medial pterygoid activity. We were interested in determining if a stable unilateral clench could be achieved through the recruitment of an ensemble of closing muscle groups with appropriately balanced activation. We performed clenching simulations with different jaw postures to investigate the effect of jaw position on the ability of the model to generate bite force.

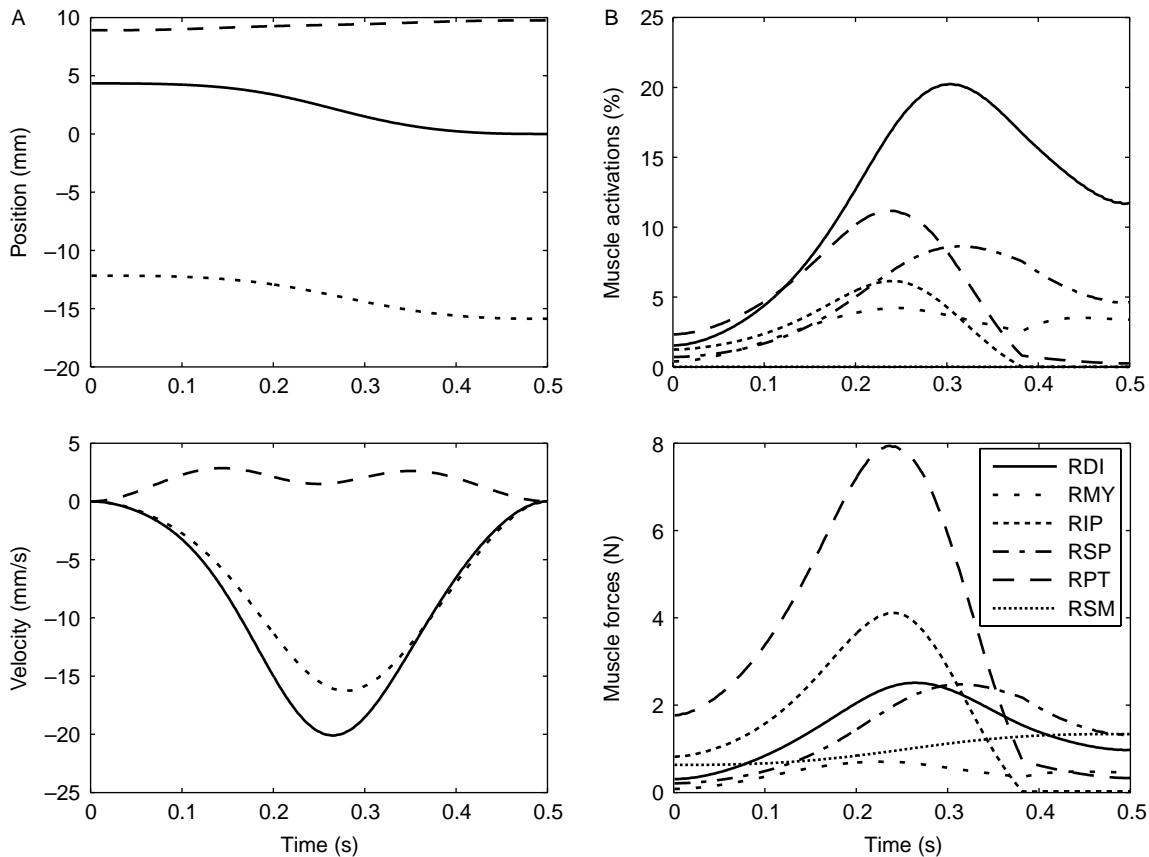


Figure 3. Movement simulation from REST (0s) to OPEN (0.5s). (A) Target position and velocity trajectories for mandibular mid-incisor point in lateral (solid lines), vertical (dotted lines) and antero-posterior directions (dashed lines). (B) Muscle activations and forces of the primary muscles used to track target trajectory.

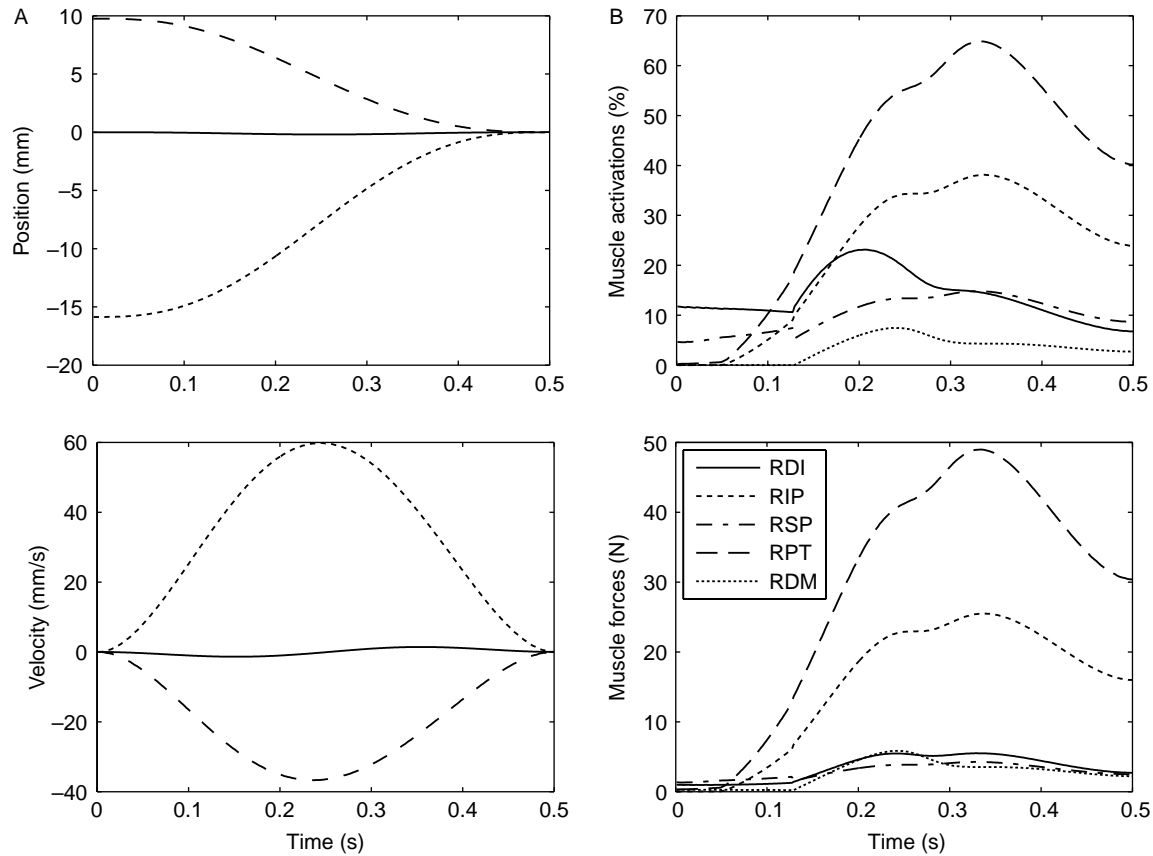


Figure 4. Movement simulation from OPEN (0s) to CLOSE (0.5s). (A) Target position and velocity trajectories for mandibular mid-incisor point in lateral (solid lines), vertical (dotted lines) and antero-posterior directions (dashed lines). (B) Muscle activations and forces of the primary muscles used to track target trajectory.

### 3. Results

#### 3.1 Deviated rest to midline retrusive open

The muscle patterns predicted by the inverse simulation for the REST-to-OPEN movement are shown in Figure 3(B) and Table 2. Incisor point movement to midline along with counter-clockwise rotation of the jaw fragment to a neutral orientation was accomplished by co-activation of the right-sided digastric and posterior temporalis muscles.

The average position error of the incisor point during the movement was 0.36, 0.22 and 0.39 mm in the left, anterior and inferior directions, respectively. Posterior temporalis inserts into the coronoid process and has a force vector best angled to apply the required torque to rotate the fragment to a symmetric midline posture. Digastric is activated to open the jaw to 20 mm as is the case in retrusive opening with an intact mandible.

Table 2. Muscle activations (%) and forces (N) for movements between REST, OPEN and CLOSE postures.

	Rest posture % (N)	Peak rest → open % (N)	Open posture % (N)	Peak open → close % (N)	Close posture % (N)
RPT	2.3 (1.8)	11.2 (7.9)	0.2 (0.3)	64.9 (49.0)	40.2 (30.4)
RSM	0.0 (0.6)	0.0 (1.3)	0.0 (1.3)	0.0 (1.3)	0.0 (0.0)
RDM	0.0 (0.2)	0.0 (0.3)	0.0 (0.3)	7.4 (5.8)	2.7 (2.2)
RMP	0.1 (0.9)	1.1 (1.9)	0.1 (1.0)	1.1 (2.0)	0.0 (0.0)
RSP	0.7 (0.2)	8.6 (2.5)	4.6 (1.3)	14.8 (4.3)	8.7 (2.5)
RIP	1.2 (0.8)	6.1 (4.1)	0.0 (0.0)	38.1 (25.5)	23.9 (16.0)
RDI	1.5 (0.3)	20.2 (2.5)	11.7 (1.0)	23.1 (5.5)	6.7 (2.7)
RMY	0.4 (0.1)	4.2 (0.7)	3.4 (0.5)	3.4 (0.5)	0.0 (0.0)

Note: Muscle force includes both passive force due to muscle stretch and active force proportional to activation.

### 3.2 Hinge closing from midline open posture

The muscle patterns predicted to move the jaw fragment along a midline hinge closing trajectory in the OPEN-to-CLOSE movement are shown in Figure 4(B) and Table 2. The average position error of the incisor point during the movement was 0.08, 0.02 and 0.03 mm in the left, posterior and inferior directions, respectively. Posterior temporalis was again recruited in order to keep the fragment at midline and its activity increased during the closing movement. Lateral pterygoids were also co-contracted, presumably to balance the lateral temporalis force and to maintain a midline movement.

### 3.3 Unilateral clench

The three simulated clenching postures are illustrated in Figure 5 and the predicted muscle activation and force magnitudes are provided in Table 3. For comparison, maximal first molar bite force for an intact mandible is within the range of 216–740 N (Waltimo and Kononen 1993). Clenching with the jaw fragment deviated towards the affected side was the most stable act. Moving towards a midline position required muscle recruitment to maintain the posture and reduced bite-force magnitudes. At 15 mm lateral and backward deviation of the mandibular mid-incisor point, the simulation was able to generate 124 N of force at the bite constraint; however, positioning the jaw medially to a 10 mm deviation reduced the bite force to 111 N and greatly increased the co-activation of opener muscles. In the midline posture, the inverse simulation with a high target bite force was unstable; however, a stable intercuspal posture was achieved with

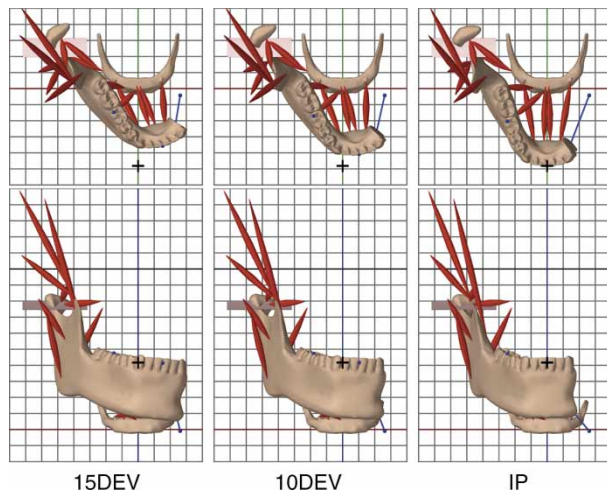


Figure 5. Horizontal and frontal-plane views of jaw postures for the different clenching tasks. The model was able to generate a 124 N bite force at 15 mm incisor deviation (15DEV); a 111 N bite force at 10 mm incisor deviation (10DEV) and a 25 N bite force at midline IP. The lower mid-incisor point at IP is denoted by +. Grid spacing is 10 mm.

Table 3. Muscle activations (%) and forces (N) for unilateral clenching simulations.

	124 N Clench at 15DEV % (N)	111 N Clench at 10DEV % (N)	25 N Clench at IP % (N)
RAT	89.9 (140.9)	90.1 (141.7)	16.3 (25.8)
RMT	0.0 (0.1)	0.0 (0.0)	4.7 (4.5)
RPT	0.0 (0.1)	0.0 (0.1)	2.8 (2.1)
RSM	16.0 (29.2)	19.3 (36.5)	6.8 (13.0)
RDM	41.9 (34.1)	86.8 (70.2)	1.2 (1.0)
RMP	88.8 (154.5)	89.0 (155.5)	11.5 (20.1)
RSP	4.5 (0.8)	15.6 (2.7)	0.3 (0.0)
RIP	5.0 (2.5)	78.0 (39.0)	5.1 (2.5)
LDI	27.2 (4.8)	14.9 (5.1)	0.0 (0.0)
RDI	44.2 (20.0)	77.5 (37.2)	0.0 (0.0)
RMY	4.7 (0.5)	2.3 (0.3)	0.0 (0.0)
LGH	5.3 (0.6)	8.3 (1.3)	0.0 (0.0)
RGH	5.7 (0.7)	8.5 (1.4)	0.0 (0.0)

Note: Muscle force includes both passive force due to muscle stretch and active force proportional to activation.

a bite force of 25 N. The main closer muscles recruited for clenching were anterior temporalis, medial pterygoid and deep masseter.

## 4. Discussion

The simulated recruitment of antagonist muscles for both free jaw movements and unilateral clenching suggests that functional deficit caused by unilateral muscle and articular loss may be at least partly overcome by stiffening the system with opposing muscles. The current simulations thus serve as a proof-of-concept of an inverse modelling approach to determine the biomechanical plausibility of hypothesised movements and associated muscle patterns in an altered jaw system. Comparison of the model predictions with patient data will require significant quantitative clinical measurements on patients.

In the reported movement simulations, the posterior temporalis was used to provide a torque to move the incisor point to the midline in a right lateral movement to compensate for the left lateral deviation caused by passive scar-tissue forces. Such a movement would normally be accomplished by the contralateral lateral pterygoids which are missing in the hemimandibulectomy case. Ipsilateral temporalis contributes to normal lateral movement (Miller 1991); therefore, it is plausible that the right-side posterior temporalis is recruited to compensate for the missing lateral pterygoid muscles in a left-sided deficit. Ipsilateral lateral pterygoids co-activate with posterior temporalis, which is atypical but necessary in the model to generate medial forces at the condyle to balance the lateral forces generated by posterior temporalis. We expect that the inclusion of lateral constraint at the joint, such as the lateral aspect of the articular fossa or the temporomandibular ligament, would reduce the need for lateral pterygoid co-activation.

Predicted muscle activations are affected by the choice of regularisation term in the optimisation (Equation (11)). Different optimality conditions have been proposed for a variety of physiological and numerical reasons (see Ait-Haddou et al. (2004) and Erdemir et al. (2007)). We use an  $\ell^2$ -norm weighted by the inverse of each muscles cross-sectional area. The main difference observed with weighted regularisation was in the relative contribution of synergistic muscles. In the lateral pterygoids, for example, the inferior-head activity was increased and superior-head activity decreased when using the weighted regulariser as compared to an unweighted  $\ell^2$ -norm, because the inferior-head is a significantly larger muscle. The relative scaling of antagonist groups was unaffected by regulariser weighting as it is prescribed by the requirements of tracking the target trajectory.

Our current tracking algorithm is formulated only for bilateral constraints. Contact modelling requires unilateral constraints that add inequality conditions on the dynamics equation of the form  $\mathbf{N}\dot{\mathbf{v}} \leq 0$  (see Fels et al. (2009)). This limitation reduces the number of tasks we can currently model: in hinge jaw opening, the condyle does not move forward off the posterior joint constraint, and in clenching the teeth are always in contact. It is possible to model contact as bilateral constraints that appear and disappear as contact is made and broken; however, this can lead to oscillating or sticking behaviour. We are investigating methods to formally include unilateral constraints in the inverse formulation.

The model currently has a number of limitations. Lacking literature on the mechanical properties of wound scarring after mandibular resection, we currently model post-operative scarring by a simplified spring element. The scar force determines the model's rest posture and, therefore, has a significant effect on muscle activations predicted to move the jaw fragment back to midline. Clinical measurements of the functional effect of scar tissue, such as jaw stiffness at different postures, are needed to adapt the scar-tissue model in an individual subject to predict subject-specific muscle activations.

The bite constraint, modelled here as a planar contact surface aligned to the occlusion plane, simulates a patient with flat teeth. Here, we found it impossible to hold a midline IP and generate a bite force more than 25 N. Moreover, all bite forces were considerably less than those normally generated in the intact jaw during tooth clenching, i.e. 216–740 N (Waltimo and Kononen 1993). A reduced capacity to generate bite force in the present case can be expected given the loss of half the closing muscles. Notwithstanding the additional, atypical contributions of antagonistic muscles made available in our simulations, the postural effect on bite-force generation reflects the extreme biomechanical conditions needed to create any significant unilateral bite force in the hemimandibulectomy patient, and it is unlikely that the eccentric jaw positions in our

study are achievable in practice. It remains possible, however, that the dental interface has a significant effect on inverse predictions of muscle activity during clenching. In future work, the shapes of the occlusal surfaces commonly used in post-surgical dental reconstruction can be incorporated in our model, making it possible to study the effects of occlusal configurations on system biomechanics and predicted muscle patterning.

To conclude, we believe that computer modelling presents a promising approach for understanding the biomechanics of surgically altered musculoskeletal systems. Inverse modelling techniques allow for systematic analysis of muscle forces rather than trial-and-error specification of input muscle patterns to a forward dynamics simulation. The inclusion of constraint forces in addition to movement targets in our inverse modelling scheme allows us to simulate dynamic clenching with the jaw model. In future studies with models of normal subjects, where simultaneous movement and EMG records are available, we hope to refine the inverse optimisation parameters and evaluate predicted muscle patterns for stereotyped movements.

## References

- Ait-Haddou R, Jinha A, Herzog W, Binding P. 2004. Analysis of the force-sharing problem using an optimization model. *Math Biosci.* 191(2):111–122.
- Buchillard S, Perrier P, Payan Y. 2009. A biomechanical model of cardinal vowel production: muscle activations and the impact of gravity on tongue positioning. *J Acoust Soc Am.* 126(4):2033–2051.
- Cottle RW, Pang JS, Stone RE. 1992. *The linear complementarity problem.* Boston (MA): Academic Press.
- Curtis D, Plesh O, Miller A, Curtis T, Sharma A, Schweitzer R, Hilsinger R, Schour L, Singer M. 1997. A comparison of masticatory function in patients with or without reconstruction of the mandible. *Head Neck.* 19(4):287–296.
- Erdemir A, McLean S, Herzog W, van den Bogert A. 2007. Model-based estimation of muscle forces exerted during movements. *Clin Biomech.* 22(2):131–154.
- Fels S, Stavness I, Hannam A, Lloyd JE, Anderson P, Batty C, Chen H, Combe C, Pang T, Mandal T, et al. 2009. Advanced tools for biomechanical modeling of the oral, pharyngeal, and laryngeal complex. *International Symposium on Biomechanics Healthcare and Information Science.*
- Hannam A, Stavness I, Lloyd J, Fels S. 2008. A dynamic model of jaw and hyoid biomechanics during chewing. *J Biomech.* 41(5):1069–1076.
- Hannam AG, Stavness I, Lloyd JE, Fels S, Miller A, Curtis D. 2010. A comparison of simulated jaw dynamics in models of segmental mandibular resection versus resection with alloplastic reconstruction. *J Prosthet Dent*, in press.
- Marunick M, Mathes B, Klein B. 1992. Masticatory function in hemimandibulectomy patients. *J Oral Rehabil.* 19(3): 289–295.
- Miller A. 1991. *Craniomandibular muscles: their role in function and form.* Boca Raton (FL): CRC-Press.
- Peck C, Langenbach G, Hannam A. 2000. Dynamic simulation of muscle and articular properties during human wide jaw opening. *Arch Oral Biol.* 45(11):963–982.

- Roumanas E, Garrett N, Blackwell K, Freymiller E, Abemayor E, Wong W, Beumer J, Fueki K, Fueki W, Kapur K. 2006. Masticatory and swallowing threshold performances with conventional and implant-supported prostheses after mandibular fibula free-flap reconstruction. *J Prosthet Dent.* 96(4): 289–297.
- Schmelzeisen R, Neukam F, Shirota T, Specht B, Wichmann M. 1996. Postoperative function after implant insertion in vascularized bone grafts in maxilla and mandible. *Plast Reconstr Surg.* 97(4):719.
- Sherif M, Gregor R, Liu L, Roy R, Hager C. 1983. Correlation of myoelectric activity and muscle force during selected cat treadmill locomotion. *J Biomech.* 16(9):691.
- Sueda S, Kaufman A, Pai DK. 2008. Musculotendon simulation for hand animation. In: *ACM SIGGRAPH '08*. New York: ACM Press. p. 1–8.
- Thelen D, Anderson F. 2006. Using computed muscle control to generate forward dynamic simulations of human walking from experimental data. *J Biomech.* 39(6):1107–1115.
- Urken M, Buchbinder D, Weinberg H, Vickery C, Sheiner A, Parker R, Schaefer J, Som P, Shapiro A, Lawson W, et al. 1991. Functional evaluation following microvascular oromandibular reconstruction of the oral cancer patient: a comparative study of reconstructed and nonreconstructed patients. *Laryngoscope.* 101(9):935–950.
- Waltimo A, Kononen M. 1993. A novel bite force recorder and maximal isometric bite force values for healthy young adults. *European J Oral Sci.* 101(3):171–175.
- Zajac F. 1989. Muscle and tendon: properties, models, scaling, and application to biomechanics and motor control. *Crit Rev Biomed Eng.* 17:359–411.